CRYSTAL GROWTH & DESIGN

Article

Cite This: *Cryst. Growth Des.* 2019, 19, 2253−2258

pubs.acs.org/crystal

Growth Study of New Complex Oxide PbO_xSe_{1-x} Thin Films by Oxygen Plasma-Assisted Molecular Beam Epitaxy

Lance L. McDowell,* Jijun Qiu, Binbin Weng, and Zhisheng Shi*

The School of Electrical and Computer Engineering, University of Oklahoma, Norman, Oklahoma, United States

ABSTRACT: In this work, we introduce the growth of a new complex oxide lead oxy-chalcogenide (PbO_xSe_{1-x}) thin film using an oxygen plasma-assisted molecular beam epitaxy method. Freshly cleaved $BaF_2(111)$ wafers were used as the substrates for this growth study. Systematic characterization of X-ray diffraction peaks, Raman shifts, absorption spectra, scanning electron microscopic imaging, and Hall measurements were conducted to elucidate the structural, optical, and electric properties of the as-grown PbO_xSe_{1-x} thin films. Specifically, X-ray diffraction measurements revealed that PbO_xSe_{1-x} films maintained the same rock-salt crystal structure as the PbSe semiconductor, but a slight shift in the lattice parameter was observed. A blue shift in the optical absorption edge also suggests that the inclusion of oxygen atoms led to the formation of a ternary compound crystal structure. Furthermore, all PbO_xSe_{1-x} thin films were observed to be polycrystalline in nature and displayed preferred [100] orientated grains. Slight variations in LO and TO phonon peak positions were also observed under Raman spectroscopy, signifying the presence of lead−oxygen bonding. This new type of complex oxide thin film has never been reported and could potentially be used to develop advanced optoelectronic devices, including mid-infrared photodetectors and light-emitting devices.

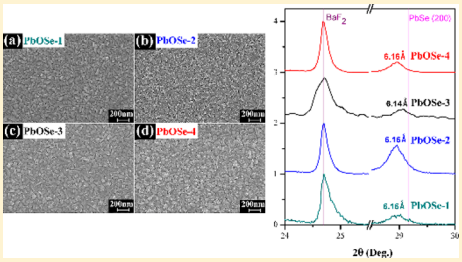

1. INTRODUCTION

Complex oxides are known to have an extraordinary wealth of electric, magnetic, optical, and mechanical properties. Applications of such material systems have found benefit in a wide range of technologies relating to energy harvesting, optical sensing, communication devices, nanoelectronics, and more.[1−4] Progress in the development of new complex oxide semiconductor material systems has also found great success in the advancement of state of the art technologies such as the growth of perovskite-type complex oxides, the indium gallium zinc oxide (INGZO) material system for flexible thin-film transistors, and bismuth vanadate ($BiVO_4$) as a complex metal oxide photoelectrode.[1,5,6] To better understand the role oxygen atoms play in the formation and properties of complex oxides, it is imperative to develop controlled methods for fabrication and characterization of such materials. For instance, lead chalcogenides, especially lead selenide (PbSe), have for a long time been a focus of interest for scientists due to having a narrow optical band gap perfectly suited for the development of optical sensors and emitters in the mid-infrared (IR) region. However, PbSe films used in such optoelectronic devices often acquire their photosensitivity from interaction with oxygen and other elements, typically through a thermal treatment called the sensitization process.[7,8] Previous studies also indicate that the PbSe interaction with oxygen results in enhanced photoluminescent properties and defect passivation, along with the formation of a $PbSeO_3$ surface layer, as well as other possible PbSe oxides.[9] However, explanations for the physical mechanisms in which PbSe interacts with oxygen to form this complex oxide semiconductor system and promote photosensitivity and enhanced photoluminescence has not yet been established without some ambiguity.[10,11] Deeper investigations into the role oxygen atoms play in the sensitization of PbSe films require a more controlled introduction of oxygen atoms and subsequent characterization of crystal formation and properties related to changes in PbSe−O_2 interactions. To the best of our knowledge, the thin film growth of lead oxy-chalcogenides has never been explored or reported. For these combined reasons, in this work, we applied molecular beam epitaxy (MBE) with the controlled inclusion of oxygen atoms via a radio frequency oxygen plasma source to study the growth of lead oxy-chalcogenide thin films systematically. Controlled substrate temperatures were used to promote high crystal quality as well as assist in PbSe−O_2 interactions. By utilizing this in situ growth method, a more uniform distribution of oxygen atoms interacting with PbSe can be accomplished in comparison to conventional postgrowth thermal oxygen treatment, which sees a large interaction rate at the surface but sharply decreases deeper into the film due to the nature of the oxygen diffusion process. Using this method, we fabricated a new complex oxide in the form of the ternary compound PbO_xSe_{1-x}. This new ternary compound complex oxide could be crucial in the understanding and future design of high-performance lead chalcogenide based complex oxide semiconductor optoelectronic devices.

2. EXPERIMENTAL METHODS

2.1. Oxygen Plasma-Assisted MBE Growth. Epitaxial PbSe was deposited by MBE on a freshly cleaved $BaF_2(111)$ substrate at a background pressure of 1×10^{-6} Pa and was used as a reference

Received: December 18, 2018
Revised: February 15, 2019
Published: February 28, 2019

DOI: 10.1021/acs.cgd.8b01872
Cryst. Growth Des. 2019, 19, 2253−2258

Table 1. Room-Temperature Properties of BaF_2, PbSe, and Common Pb Oxides and PbSe Oxides

material	crystal structure	lattice constant (Å)	thermal expansion (K^{-1})	band gap (eV)
BaF_2	cubic (fluorite)	6.196	1.84×10^{-5}	11
PbSe	cubic (rock salt)	6.124	1.94×10^{-5}	0.27 (direct)[12]
PbO	tetragonal	a = 4.06	$a_o = 5.2 \times 10^{-6}$ [13]	1.9 (indirect)[14]
		c = 5.51	$c_o = 8.3 \times 10^{-6}$	
	orthorhombic	a = 5.8931	a_o, $c_o = 3.1 \times 10^{-6}$ [15]	2.7 (indirect)[16]
		b = 5.4904	$b_o = 9.8 \times 10^{-6}$	
		c = 4.7528		
$PbSeO_3$	monoclinic	a = 4.5437		3.17 (direct)[17]
		b = 5.5137		
		c = 6.6340		
$PbSeO_4$	orthorhombic	a = 8.5800		3.17 (indirect)[18]
		b = 5.6300		
		c = 7.1200		

sample for subsequent growths. BaF_2 substrates were utilized for their excellent long-wave optical transmittance and electrical insulation, allowing for both optical and electrical characterization to be carried out. Furthermore, BaF_2 substrates share similar cubic crystal structures, lattice parameters, and coefficients of thermal expansion with PbSe, whose relevant material parameters are provided in Table 1.

Subsequently, PbSe evaporation via an effusion cell was performed on the freshly cleaved BaF_2(111) substrates under various conditions utilizing an rf oxygen plasma atom source. Oxygen background pressures of 5×10^{-3} and 9×10^{-3} Pa were achieved with oxygen flow rates of 0.8 and 1.4 sccm, respectively. The incursive oxygen molecules were ionized under an rf mode inductively coupled plasma process at 250 W. The resultant films were deposited at substrate temperatures of 350 and 420 °C for 1 h, resulting in 1 μm thick thin films, which are described in Table 2.

Table 2. Growth Parameters of PbO_xSe_{1-x} Thin Films

sample	substrate temperature (°C)	oxygen flow rate (sccm)	ionization power (W)
PbOSe-1	350	0.8	250
PbOSe-2	350	1.4	250
PbOSe-3	420	0.8	250
PbOSe-4	420	1.4	250

While Pb oxides and PbSe oxides have been previously characterized, oxygen plasma-assisted MBE growth of PbSe(O_x) films has never been studied. In addition to providing a list of relevant material properties for BaF_2 and PbSe, Table 1 also includes information on some of the previously reported Pb oxides and PbSe oxides which may have been expected to form under the stated growth conditions. However, subsequent characterization of deposited thin films utilizing the compound PbSe effusion cell and rf oxygen plasma source indicated the formation of a new ternary PbO_xSe_{1-x} complex oxide. The surface morphology of PbO_xSe_{1-x} films was investigated by scanning electron microscopy (SEM), while a Bruker Fourier transform infrared spectroscopy (FTIR) apparatus operating in the mid-infrared (mid-IR) spectral range was used to characterize their optical properties. Electrical properties of PbO_xSe_{1-x} films were studied by performing Hall effect measurements at room temperature. High-resolution X-ray diffraction (XRD) analyses were performed using a Rigaku Ultima IV diffractometer. Cu Kα radiation (40 kV, 44 mA) was used in parallel beam mode, and data analysis was completed using the MDI Jade2010 software with the ICDD (International Centre for Diffraction Data) PDF4+ database. Long-wave LO and TO phonon modes were investigated with a Renishaw inVia Raman microscope, illuminated by a 532 nm 500 mW green laser excitation source.

3. RESULTS AND DISCUSSION

3.1. Film Morphology and Composition. SEM images of all PbO_xSe_{1-x} thin films reveal the formation of a polycrystalline structure with densely packed grains, as shown in Figures 1 and 2. Observing the surface morphology

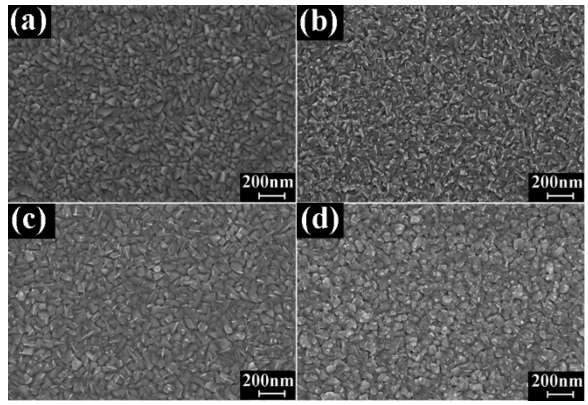

Figure 1. SEM surface images for (a) PbOSe-1, (b) PbOSe-2, (c) PbOSe-3, (d) and PbOSe-4, thin films.

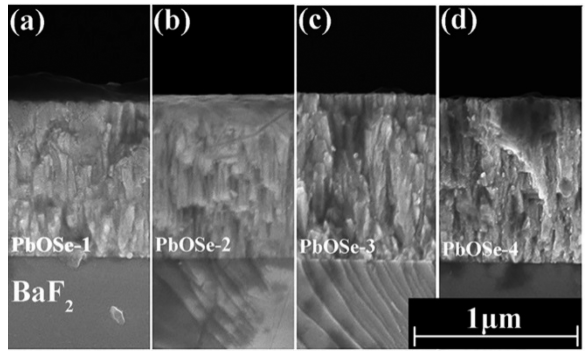

Figure 2. SEM cross section images of (a) PbOSe-1, (b) PbOSe-2, (c) PbOSe-3, (d) and PbOSe-4 thin films.

of PbO_xSe_{1-x} thin films in Figure 1 reveals the presence of [100] and [111] orientated grains. Cross-section SEM images in Figure 2 display the polycrystalline nature of PbO_xSe_{1-x} thin films grown with high packing density, smooth surface, good adhesion to the substrate, and uniform thickness between growths. Figure 3 serves as an aid for visualizing the difference

DOI: 10.1021/acs.cgd.8b01872
Cryst. Growth Des. 2019, 19, 2253−2258

in surface morphologies of [100] and [111] cubic lattice structures.

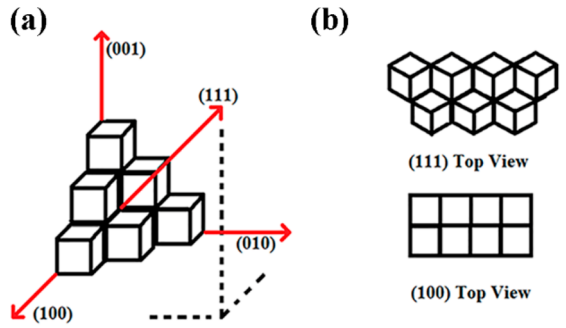

Figure 3. Visual schematic for cubic crystal orientation about the (a) point of origin given coordinates (x, y, z) and (b) top view of the cubic crystal structure.

PbO_xSe_{1-x} films deposited at low oxygen flow rates (i.e., PbOSe-1 and PbOSe-3) contained mixed [111] and [100] oriented grains, while PbO_xSe_{1-x} films deposited at a higher oxygen flow rate showed preferred [100] oriented grains. The crystal growth for PbO_xSe_{1-x} films differed from that of the reference PbSe sample, which grew [111] single crystals on the nearly lattice and thermal expansion matched BaF_2(111) substrate. This result suggests that the growth mechanism for PbO_xSe_{1-x} thin films relies heavily on the influence of oxygen overpressure in the growth chamber. As per our reference sample, PbSe films deposited by MBE on BaF_2(111) substrates typically grow epitaxially along the [111] direction. However, the presence of oxygen atoms on the growth surface, along with increased atomic scattering from the low vacuum environment during PbO_xSe_{1-x} deposition, seems to have altered the nucleation process during crystal formation. As a result, this led to island growth with the presence of varying oriented grains. Although the formation of [111] oriented grains is typically preferred due to the closely lattice matched BaF_2(111) substrate, competition for the [100] orientation now exists due to changes in surface and strain energy relations between neighboring grains for the polycrystalline films. This phenomenon has been previously reported by Sun et al., where calculations of surface and strain energy densities for the physical deposition of polycrystalline PbSe films revealed a lower energy of formation for [100] oriented grains at substrate temperatures >250 °C.[19] Therefore, it is expected that polycrystalline growth of a PbSe-like rock-salt structure, such as our PbO_xSe_{1-x} thin films, would result in the formation of [100] oriented grains at high substrate temperature deposition. In conjunction with SEM analysis, energy-dispersive X-ray spectroscopy (EDX) was employed in hopes of determining the oxygen x concentration of PbO_xSe_{1-x} thin films, resulting in x values in the range x = 0.2−0.35. However, the resolving power of the EDX measurement did not allow for a distinction between contributions of elemental composition in crystal grains versus grain boundaries that exist in the polycrystalline PbO_xSe_{1-x} thin films. Due to the overpressure of oxygen in the growth chamber, as well as prolonged exposure to the atmosphere postgrowth, large amounts of oxygen atoms may have diffused or embedded themselves in the film via grain boundaries or defect centers. Similar phenomena have been reported previously, where lead-rich n-type PbSe films converted to p-type after prolonged exposure to the atmosphere.[20] Researchers concluded that the PbSe interaction with oxygen in the air resulted in the diffusion and incorporation of oxygen atoms into the film, producing the flip from n-type to p-type carrier concentration. These processes may have contributed to the overestimation of x contained in the active PbO_xSe_{1-x} lattice structure by EDX measurements, due to oxygen interstitials and oxygen gas trapped in the grain boundaries during crystal formation and postgrowth exposure to air. Therefore, EDX results could not be used to accurately determine oxygen composition. Further studies using other techniques to determine the oxygen composition will be performed in the future.

3.2. X-ray Diffraction. Parallel beam XRD analysis of PbO_xSe_{1-x} thin films, as shown in Figure 4, reveal a rock-salt

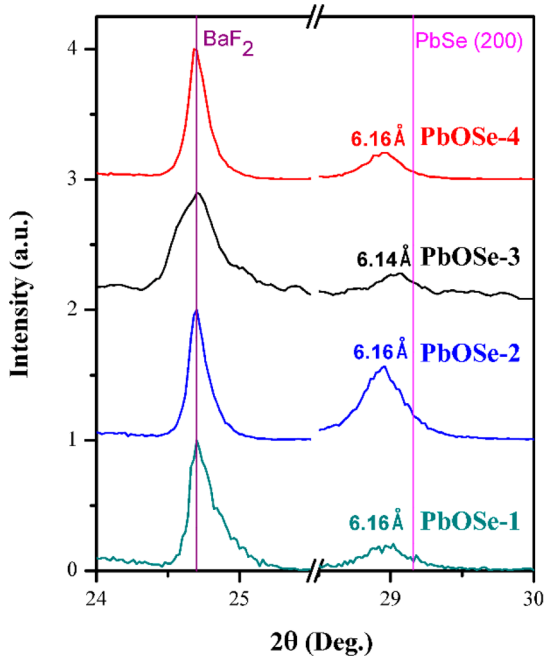

Figure 4. XRD spectra for PbO_xSe_{1-x} thin films.

crystal structure with preferred (200) peak contribution, along with possible (111) peaks masked by the BaF_2(111) substrate peak. Investigations of XRD peak intensity and symmetry, along with full width half-maximum (fwhm) values of PbO_xSe_{1-x}(200) peaks and slight lattice constant shifts, provide possible explanations for crystal formation and structure when they are compared with SEM images and reference PbSe films.

No peak contributions from the previously reported PbO, $PbSeO_3$, or $PbSeO_4$ were observed. However, a slight shift in the lattice parameter for deposited films was apparent given the offset in the PbO_xSe_{1-x}(200) peak positions relative to PbSe. Since the (200) peak belongs exclusively to the PbO_xSe_{1-x} film, the measured 2θ shifts to lower angles from the reference PbSe(200) peak position signify an increase in lattice constant. While PbSe has a rock-salt structure with a lattice constant of a = 6.12 Å, PbO_xSe_{1-x} films produced a slight lattice constant shift, as shown in Table 3, in the range a = 6.14−6.16 Å. While previous studies of Pb−O bonding report shortened bond lengths in comparison with Pb−Se bonds, XRD analysis suggests the ternary Pb−O−Se complex oxide forms an overall larger lattice constant in comparison with conventional PbSe films.

DOI: 10.1021/acs.cgd.8b01872
Cryst. Growth Des. 2019, 19, 2253−2258

Table 3. Lattice Parameters and fwhm Values of PbSe and PbO_xSe_{1-x} Thin Films

film	lattice constant (Å)	PbO_xSe_{1-x}(200) fwhm (arcsec)
reference epitaxial PbSe	6.12	
PbOSe-1	6.16	487.8
PbOSe-2	6.16	478.8
PbOSe-3	6.14	369.0
PbOSe-4	6.16	392.4

Since we observe shifting of the (200) peak position to lower 2θ angles, we should expect to see shifting of the (111) peak position to lower angles as well. However, this would make any PbO_xSe_{1-x}(111) peak contributions almost entirely overlapped with the BaF_2(111) substrate peak, making the PbO_xSe_{1-x}(111) film peak difficult to analyze. For this reason, we speculate that peak broadening and asymmetry of the BaF_2(111) substrate peak is possibly linked to an increase in the presence of a PbO_xSe_{1-x}(111) peak contribution. This effect is more pronounced in the low oxygen flow rate PbOSe-1 and PbOSe-3 samples, along with a reduction in the (200) peak intensity. In this case, XRD peak contributions coincide with observations made during SEM analysis, in which lower oxygen flow rates produced PbO_xSe_{1-x} crystal films with lower (200) vs (111) ratios. Table 3 also includes an investigation of the full width half-maximum (fwhm) values of PbO_xSe_{1-x}(200) XRD peaks. According to Scherrer's equation, the larger measured fwhm values found in PbOSe-1 and PbOSe-2 suggest the formation of smaller grain sizes in comparison to the high substrate temperature growths, which is also observed in top-down SEM images in Figure 1.

3.3. Raman Spectroscopy. Raman spectra of the reference PbSe film reveals characteristic PbSe longitudinal and transverse optical phonons, which have been previously reported in similar MBE grown PbSe films.[21] Figure 5 shows that, for PbO_xSe_{1-x} films, singular peaks at the LO, 2LO, and 2TO peak positions were present, while no individual phonon mode contribution from either PbSe or PbO was detected.

This indicates that there is no separated PbSe or Pb oxide phase present in the film, further supporting that a ternary PbO_xSe_{1-x} crystal structure has been formed. Subsequently, PbO_xSe_{1-x} films show similar PbSe-like profiles, but with slight variations in LO, 2LO, and 2TO phonon peak positions. Raman shifts of PbO_xSe_{1-x} films reveal a shifting of LO and 2LO phonon peak positions to higher wavenumbers in comparison with the reference PbSe film. The LO phonon mode contains the highest intensity for all deposited films, with increasing wavenumber for each subsequent PbO_xSe_{1-x} sample ranging from 0.7% up to a maximum of 4.4%. On comparison of the previous investigations into Raman shift for PbO films given in Table 4, our PbO_xSe_{1-x} thin films experienced a Raman shift between those of PbSe and PbO. As a ternary compound, the PbO_xSe_{1-x} Raman shift is the result of a ratio between lead−selenium and lead−oxygen bonding, where a Raman shift approaching that of characteristic PbO phonon modes is a result of increasing oxygen concentration, producing more lead−oxygen bonds. The largest difference in Raman shift was observed for the PbOSe-2 film deposited at the lower 350 °C substrate temperature and higher 1.4 sccm oxygen flow rate. Conversely, the PbOSe-3 film deposited at the higher 420 °C substrate temperature and lower 0.8 sccm oxygen flow rate resulted in the smallest difference from

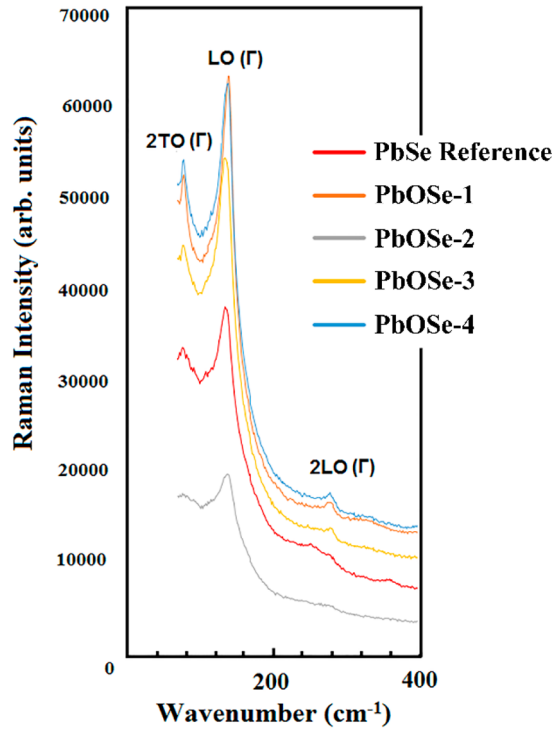

Figure 5. Raman spectra of PbO_xSe_{1-x} films.

Table 4. Peak Positions of 2TO, LO, and 2LO Phonon Modes in PbO_xSe_{1-x} Films

sample	2TO (cm^{-1})	LO (cm^{-1})	2LO (cm^{-1})
PbSe reference	79	136	271
PbO tetragonal	81	145.5	337
PbO orthorhombic	71.5	143	289.5
PbOSe-1	80	141	280
PbOSe-2	80	142	283
PbOSe-3	79	137	273
PbOSe-4	80	138	278

characteristic PbSe LO, 2LO, and 2TO phonon peak positions. It has been previously reported that the Raman shift $\Delta\omega$ varies depending on composition and temperature effects as they relate to bond length and energy and may be represented by the equation[22]

$$\Delta\omega \propto \frac{zE_b(z)^{1/2}}{d(z)} \quad (1)$$

where z is the atomic coordination number and $d(z)$ and $E_b(z)$ are the bond length and energy, respectively. A comparison of crystal films measured at the same ambient temperature reveals an increase in Raman shift due to either a decrease in bonding length or an increase in bonding energy resulting from differences in composition. Although XRD measurements revealed a slight increase in bonding length of +0.02−0.04 Å for PbO_xSe_{1-x} films in comparison with PbSe, the Raman shift indicated an increase rather than a decrease in $\Delta\omega$. This is likely due to the reported energy difference of Pb−O bonds and Pb−Se bonds, where the Pb−Se bond (302.9 ± 4 kJ mol^{-1}) requires less energy to be broken than the Pb−O (382.0 ± 12.6 kJ mol^{-1}) and Se−O (464.8 ± 21.3 kJ mol^{-1}) bonds.[23] The energy relation between these bonds suggests that the inclusion of oxygen atoms during crystal formation

DOI: 10.1021/acs.cgd.8b01872
Cryst. Growth Des. 2019, 19, 2253−2258

more readily breaks the Pb−Se bond to form higher energy Pb−O and possibly Se−O and Pb−O−Se chain bonds.

3.4. Optical Properties. Figure 6 depicts the absorption spectra of PbO_xSe_{1-x} films measured by FTIR, which revealed

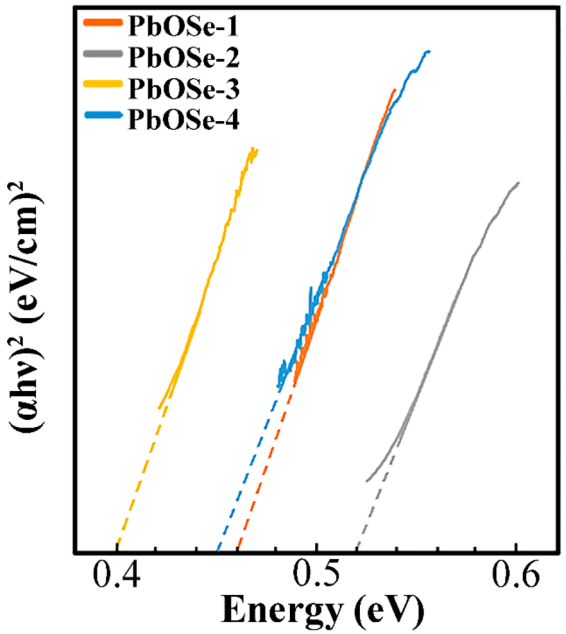

Figure 6. Band gap determination of PbO_xSe_{1-x} thin films.

a blue shift in the optical band gap in comparison with the reference PbSe sample. The band gap energies provided in Table 5 show that the optical absorption edge of PbO_xSe_{1-x} thin films resulted in a blue shift ranging from +48% to +89% relative to the reference PbSe film.

Table 5. Measured Optical Band Gaps for PbSe and PbO_xSe_{1-x} Films

sample	band gap (direct, eV)
epitaxial PbSe	0.27
PbOSe-3	0.4
PbOSe-4	0.45
PbOSe-1	0.46
PbOSe-2	0.51

It is important to note that the PbOSe-2 thin film, which contained the largest difference in Raman shift, also resulted in the largest blue shift of the optical band gap in comparison to the reference PbSe film. Conversely, the PbOSe-3 film, which contained the smallest difference in Raman shift, also resulted in the smallest blue shift of the optical band gap. This suggests a trend in which property changes associated with enhanced oxygen atom incorporation during crystal formation result from both the lower 350 °C substrate temperature and an increased oxygen flow rate during deposition.

3.5. Electrical Properties. Electrical properties of PbO_xSe_{1-x} films grown under varying conditions are shown in Table 6.

Hall effect measurements reveal that all PbO_xSe_{1-x} films are dominated by hole transport, with increasing p-type carrier concentration ranging from 1.79×10^{18} to 1.26×10^{19} cm^{-3} observed for films grown with increasing oxygen flow rate. Conversely, the carrier mobility decreases with increasing oxygen flow rate, pointing toward possible increases in impurity scattering, carrier scattering, alloy scattering, and grain boundary scattering. On comparison of Hall measurements with SEM, XRD, and band gap shift, the largest decrease in mobility observed in PbOSe-2 may be explained by contributions of all the above mechanisms. For example, the large fwhm of PbOSe-2 implies a smaller crystal size, which is also observed in the SEM image in Figure 1, resulting in increased boundary scattering of carriers at grain−grain interfaces. Further, the carrier concentration of the PbOSe-2 film was the highest of all PbO_xSe_{1-x} thin films, almost 1 order of magnitude higher than that for PbOSe-1, leading to the potential for heavy carrier scattering. PbOSe-2 also had the largest band gap shift from PbSe resulting from increased oxygen atom incorporation, potentially increasing alloy scattering and further reducing carrier mobility. Other PbO_xSe_{1-x} films may be similarly affected by these mechanisms; however, PbOSe-2 displays the largest decrease in mobility due to having the highest oxygen atom incorporation along with smaller relative grain size. Previous reports of ternary compounds such as $PbSr_xSe_{1-x}$ and $PbEu_xTe_{1-x}$ have been used to increase the band gap energy for IV−VI Pb salt based semiconductor optoelectronic devices to be used as electrical confinement layers.[24,25] In doing so, the mobility decreased exponentially with Sr or Eu composition in comparison to PbSe. The p-type doping concentration in such ternary compounds is also limited, as it is not possible to achieve high doping concentrations close to 1.0×10^{19} cm^{-3}. This new PbO_xSe_{1-x} ternary compound has succeeded in forming a larger band gap, nearly the same lattice constant as PbSe, and high p-type doping concentration. This, plus the positive role of defect passivation, may make this new PbO_xSe_{1-x} complex oxide attractive for PbSe-related optoelectronic devices. The band alignment with PbSe will need to be studied for future applications.

4. CONCLUSION

The growth of new ternary complex oxy-chalcogenide PbO_xSe_{1-x} thin films has been reported here, along with the characterization of optical, electrical, and crystallographic properties associated with changes in growth parameters. The trend follows from our experiments that film property changes due to increased oxygen concentration were enhanced by both the increased oxygen flow rate (1.4 sccm) and the lower substrate temperature (350 °C) in the 350−420 °C range. The potential application of such PbO_xSe_{1-x} thin films could find benefit in both band gap tuning and p-type doping

Table 6. Electrical Properties of PbO_xSe_{1-x} Thin Films

	sample			
	PbOSe-1	PbOSe-2	PbOSe-3	PbOSe-4
carrier concentration (cm^{-3})	1.79×10^{18}	1.26×10^{19}	3.13×10^{18}	9.82×10^{18}
carrier mobility (cm^2 V^{-1} s^{-1})	53.19	0.42	11.95	3.95

DOI: 10.1021/acs.cgd.8b01872
Cryst. Growth Des. 2019, 19, 2253−2258

of PbSe material systems, as well as furthering the understanding and future design of high-performance PbSe based complex oxide semiconductor optoelectronic devices. Further study of the growth mechanism along with changes in optical and electrical properties for PbO_xSe_{1-x} thin films would provide improved control of physical properties on PbSe-based systems, leading to an enhanced design of PbSe-based optoelectronic devices.

AUTHOR INFORMATION

Corresponding Authors

*E-mail for L.L.M.: lance.l.mcdowell-1@ou.edu.

*E-mail for Z.S.: shi@ou.edu.

ORCID

Lance L. McDowell: 0000-0003-2069-994X

Jijun Qiu: 0000-0002-2537-5250

Notes

The authors declare no competing financial interest.

ACKNOWLEDGMENTS

This work was supported by the US Army Research Office (ARO) under Contract No. W911NF-18-1-0418.

REFERENCES

(1) Rettie, A. J.; Lee, H. C.; Marshall, L. G.; Lin, J. F.; Capan, C.; Lindemuth, J.; McCloy, J. S.; Zhou, J.; Bard, A. J.; Mullins, C. B. Combined Charge Carrier Transport and Photoelectrochemical Characterization of BiVO4 Single Crystals: Intrinsic Behavior of a Complex Metal Oxide. *J. Am. Chem. Soc.* **2013**, *135*, 11389−11396.

(2) Lee, J.; Zhu, H.; Yadav, G. G.; Caruthers, J.; Wu, Y. Porous ternary complex metal oxide nanoparticles converted from core/shell nanoparticles. *Nano Res.* **2016**, *9*, 996−1004.

(3) Zhang, L.; Zhou, Y.; Guo, L.; Zhao, W.; Barnes, A.; Zhang, H. T.; Eaton, C.; Zheng, Y.; Brahlek, M.; Haneef, H. F.; Podraza, N. J.; Chan, M. H. W.; Gopalan, V.; Rabe, K. M.; Herbert, R. E. Correlated metals as transparent conductors. *Nat. Mater.* **2016**, *15*, 204−210.

(4) Jia, Q. X.; McCleskey, T. M.; Burrell, A. K.; Lin, Y.; Collis, G. E.; Wang, H.; Li, A. D. Q.; Foltyn, S. R. Polymer-assisted deposition of metal-oxide films. *Nat. Mater.* **2004**, *3*, 529−532.

(5) Habermeier, H. U. Thin films of perovskite-type complex oxides. *Mater. Today* **2007**, *10*, 34−43.

(6) Nomura, K.; Ohta, H.; Takagi, A.; Kamiya, T.; Hirano, M.; Hosono, H. Room-temperature fabrication of transparent flexible thin-film transistors using amorphous oxide semiconductors. *Nature* **2004**, *432*, 488−492.

(7) Munoz, A.; Melendez, J.; Torquemada, M. C.; Rodrigo, M. T.; Cebrian, J.; de Castro, A. J.; Meneses, J.; Ugarte, M.; Lopez, F.; Vergara, G.; Hernandez, J. L.; Martin, J. M.; Adell, L.; Montojo, M. T. PbSe Photodetector Arrays for IR Sensors. *Thin Solid Films* **1998**, *317*, 425.

(8) Qiu, J.; Weng, B.; Yuan, Z.; Shi, Z. Study of sensitization process on mid-infrared uncooled PbSe photoconductive detectors leads to high detectivity. *J. Appl. Phys.* **2013**, *113*, 103102.

(9) Zhao, F.; Mukherjee, S.; Ma, J.; Li, D.; Elizondo, S. L.; Shi, Z. Influence of oxygen passivation on optical properties of PbSe thin films. *Appl. Phys. Lett.* **2008**, *92*, 211110.

(10) Zhao, L.; Qiu, J.; Weng, B.; Chang, C.; Yuan, Z.; Shi, Z. Understanding sensitization behavior of lead selenide photoconductive detectors by charge separation model. *J. Appl. Phys.* **2014**, *115*, 084502.

(11) Weng, B.; Qiu, J.; Zhao, L.; Yuan, Z.; Chang, C.; Shi, Z. Recent development on the uncooled mid-infrared PbSe detectors with high detectivity. *Proc. SPIE* **2014**, 899311.

(12) Ekuma, C. E.; Singh, D. J.; Moreno, J.; Jarrell, M. Optical Properties of PbTe and PbSe. *Phys. Rev. B: Condens. Matter Mater. Phys.* **2012**, *85*, 085205.

(13) Sorrell, C. A. Thermal Expansion of Tetragonal PbO. *J. Am. Ceram. Soc.* **1970**, *53*, 641−644.

(14) Berashevich, J.; Semeniuk, O.; Rowlands, J. A.; Reznik, A. Anisotropy of the carrier effective masses in bulk α-PbO. *EPL* **2012**, *99*, 47005.

(15) Sorrell, C. A. Thermal Expansion of Orthorhombic PbO. *J. Am. Ceram. Soc.* **1970**, *53*, 552−554.

(16) Iinuma, K.; Seki, T. Optical Absorption Coefficients of Lead Monoxide Single Crystal of the Yellow Modification. *Mater. Res. Bull.* **1967**, *2*, 527−532.

(17) Tomaev, V. V.; Smolyaninov, V. D.; Stoyanova, T. V.; Egorov, S. V. Preparation of $PbSeO_3$ as a New Material, Sensitive to the Electromagnetic Radiation in UV Range. *J. Phys.: Conf. Ser.* **2016**, *741*, 012036.

(18) Errandonea, D.; Muñoz, A.; Rodríguez-Hernández, P.; Proctor, J. E.; Sapiña, F.; Bettinelli, M. Theoretical and Experimental Study of the Crystal Structures, Lattice Vibrations, and Band Structures of Monazite-Type PbCrO4, PbSeO4, SrCrO4, and SrSeO4. *Inorg. Chem.* **2015**, *54*, 7524−7535.

(19) Sun, X.; Gaoa, K.; Pang, X.; Yang, H.; Volinsky, A. A. Study on the growth mechanism and optical properties of sputtered lead selenide thin films. *Appl. Surf. Sci.* **2015**, *356*, 978−985.

(20) Kazantsev, D. V.; Selivanov, Y. G.; Trofimov, V. T.; Chizhevskii, E. G. Surface States of Lead Selenide Crystals. *AIP* **1995**, *62* (5), 422−426.

(21) Kuzivanov, M. O.; Zimin, S. P.; Fedorov, A. V.; Baranov, A. V. Raman Scattering in Lead Selenide Films at a Low Excitation Level. *Opt. Spectrosc.* **2015**, *119*, 938−942.

(22) Yang, X.; Liu, Y.; Liu, X. J.; Peng, J. Z.; Zhao, H.; Sun, C. Q. Composition and Temperature-Resolved Raman Shift of Silicon. *Appl. Spectrosc.* **2018**, *72*, 598−603.

(23) Gautier, C.; Cambon-Muller, M.; Averous, M. Study of PbSe layer oxidation and oxide dissolution. *Appl. Surf. Sci.* **1999**, *141*, 157−163.

(24) Yang, H. F.; Shen, W. Z.; Pang, Q. J. Study of photocurrent characteristics in PbSrSe thin films for infrared detection. *Appl. Phys. Lett.* **2002**, *81*, 2394.

(25) Partin, D. L. Lead Salt Quantum Effect Structures. *IEEE J. Quantum Electron.* **1988**, *24*, 1716−1726.

DOI: 10.1021/acs.cgd.8b01872
Cryst. Growth Des. 2019, 19, 2253−2258